NeuroImage: Clinical 19 (2018) 174–181

Contents lists available at ScienceDirect

NeuroImage: Clinical

journal homepage: www.elsevier.com/locate/ynicl

# Quantitative analysis of neurite orientation dispersion and density imaging in grading gliomas and detecting *IDH-1* gene mutation status

Jing Zhao[a,1], Ji-bin Li[b,1], Jing-yan Wang[a], Yu-liang Wang[a], Da-wei Liu[c], Xin-bei Li[a], Yu-kun Song[a], Yi-su Tian[a], Xu Yan[d], Zhu-hao Li[a], Shao-fu He[a], Xiao-long Huang[e], Li Jiang[a], Zhi-yun Yang[a], Jian-ping Chu[a,*]

[a] Department of Radiology, The First Affiliated Hospital, Sun Yat-Sen University, 58, The Second Zhongshan Road, Guangzhou, Guangdong 510080, China
[b] Department of Clinical Research, Sun Yat-sen University Cancer Center, 651, Dong Feng Dong Lu Road, Guangzhou, Guangdong 510060, China
[c] Department of Pathology, The First Affiliated Hospital, Sun Yat-Sen University, 58, The Second Zhongshan Road, Guangzhou, Guangdong 510080, China
[d] MR Collaboration NE Asia, Siemens Healthcare 278, Zhou Zhu Road, Nanhui, Shanghai 201318, China
[e] Department of Neurology, Sun Yat-Sen Memorial Hospital, Sun Yat-Sen University, 33, Ying Feng Lu Road, Hai Zhu district, Guangzhou, Guangdong 510235, China

ARTICLE INFO

*Keywords:*
Glioma
Magnetic Resonance Imaging
Diffusion
Genes
Isocitrate dehydrogenase

ABSTRACT

*Background and purpose:* Neurite orientation dispersion and density imaging (NODDI) is a new diffusion MRI technique that has rarely been applied for glioma grading. The purpose of this study was to quantitatively evaluate the diagnostic efficiency of NODDI in tumour parenchyma (TP) and peritumoural area (PT) for grading gliomas and detecting isocitrate dehydrogenase-1 (*IDH-1*) mutation status.

*Methods:* Forty-two patients (male: 23, female: 19, mean age: 44.5 y) were recruited and underwent whole brain NODDI examination. Intracellular volume fraction (icvf) and orientation dispersion index (ODI) maps were derived. Three ROIs were manually placed on TP and PT regions for each case. The corresponding average values of icvf and ODI were calculated, and their diagnostic efficiency was assessed.

*Results:* Tumours with high $icvf_{TP}$ ($\geq 0.306$) and low $icvf_{PT}$ ($\leq 0.331$) were more likely to be high-grade gliomas (HGGs), while lesions with low $icvf_{TP}$ ($< 0.306$) and high $icvf_{PT}$ ($> 0.331$) were prone to be low-grade gliomas (LGGs) ($P < 0.001$). A multivariate logistic regression model including patient age and icvf values in TP and PT regions most accurately predicted glioma grade (AUC = 0.92, $P < 0.001$), with a sensitivity and specificity of 92% and 89%, respectively. However, no significant differences were found in NODDI metrics for differentiating *IDH-1* mutation status.

*Conclusions:* The quantitative NODDI metrics in the TP and PT regions are highly valuable for glioma grading. A multivariate logistic regression model using the patient age and the icvf values in TP and PT regions showed very high predictive power. However, the utility of NODDI metrics for detecting *IDH-1* mutation status has not been fully explored, as a larger sample size may be necessary to uncover benefits.

## 1. Introduction

Gliomas account for approximately 30% of all brain and central nervous system tumours and 80% of all malignant brain tumours (Goodenberger & Jenkins, 2012). Accurate preoperative localization, diagnosis, and grading are highly important for proper treatment planning and selection in all phases of glioma. Diffusion-weighted imaging (DWI) is increasingly used as an imaging biomarker for the detection and characterization of gliomas as well as for prognostication and monitoring treatment response. The unique advantages of this technique make it well-poised to answer questions about tumour biology at a cellular level as well as the microstructure of peritumoural white matter (White et al., 2014).

Advanced diffusion techniques, such as diffusion tensor imaging (DTI) and diffusion kurtosis imaging (DKI), have been widely used for glioma grading, and their diagnostic efficiency has gradually improved (Tropine et al., 2004; Bai et al., 2016). Newly developed neurite orientation dispersion and density imaging (NODDI) is an advanced

*Abbreviations:* NODDI, neurite orientation dispersion and density imaging; TP, tumour parenchyma; PT, peritumoural area; icvf, intracellular volume fraction; ODI, orientation dispersion index; 2-HG, 2-hydroxyglutarate; NAWM, contralateral normal-appearing white matter

* Corresponding author.
*E-mail address:* chujping@mail.sysu.edu.cn (J.-p. Chu).
[1] Contributed equally (first author: Jing Zhao, co-first author: Ji-bin Li).

https://doi.org/10.1016/j.nicl.2018.04.011
Received 26 October 2017; Received in revised form 26 March 2018; Accepted 9 April 2018
Available online 12 April 2018

diffusion technique that assumes a three-compartment biophysical tissue model, including intracellular, extracellular, and cerebrospinal fluids within a single voxel. This technique enables inference and quantification of the direction and structure of neurites (axons and dendrites) and provides valuable insights about tumour physiology (Zhang et al., 2012). The representative parameters of NODDI are intracellular volume fraction (icvf) and orientation dispersion index (ODI). Recently, NODDI has been applied to analyse stroke (Adluru et al., 2014), focal cerebral cortical dysplasia (Winston et al., 2014) and Parkinson's disease (Kamagata et al., 2016). Furthermore, Wen et al. (Wen et al., 2015) determined the feasibility of NODDI for characterizing gliomas with multiband echo planner imaging in 7 T MRI, and found that, similar to 3 T MRI, the data quality was clinically acceptable. To date, NODDI has rarely been applied for grading gliomas.

The 2016 World Health Organization Classification of Tumours in the Central Nervous System, for the first time, uses molecular parameters and histology to define many tumour entities (Louis et al., 2016). The most prominent change is that the new edition incorporates the status of isocitrate dehydrogenase (*IDH*) into glioma diagnosis, with the majority of *IDH* mutations being *IDH-1* positive (Hartmann et al., 2009). Regardless of glioma grade, patients with *IDH-1* positive mutations have a better chance of survival (Hartmann et al., 2009; Weller et al., 2013; Hartmann et al., 2010; Weiler & Wick, 2012). Currently, magnetic resonance spectroscopy (MRS) can be used to determine the mutation status of *IDH* by detecting the 2-hydroxyglutarate (2-HG) level because *IDH-1*-positive gliomas express more 2-HG than *IDH-1*-negative gliomas (Andronesi et al., 2013; Bertolino et al., 2014). However, accurate detection of the 2-HG concentration by MRS is highly dependent on the magnetic field intensity, and high false positivity rates limit its clinical application (Bertolino et al., 2014). In addition, some studies have applied dynamic susceptibility contrast MRI (DSC-MR), DTI, DKI and DWI for non-invasive assessment of *IDH-1* mutation status with promising results (Kickingereder et al., 2015; Lee et al., 2015; Xiong et al., 2016; Hempel et al., 2017a; Hempel et al., 2017b). Their results showed that patients with *IDH-1* mutations have higher apparent diffusion coefficient (ADC) values but lower mean kurtosis (MK), fractional anisotropy (FA) and relative cerebral blood volumes. However, the utility of NODDI for detecting *IDH-1* mutation status is unknown.

Therefore, the purpose of this study was to assess the value of NODDI metrics (icvf and ODI) in grading gliomas and detecting *IDH-1* mutation status.

## 2. Materials and methods

### 2.1. Patients

This study was approved by the Research Ethics Committee of The First Affiliated Hospital of Sun Yat-sen University according to the ethical guidelines for human research and is compliant with the Health Insurance Portability and Accountability Act (HIPAA). Written informed consent was obtained from adult patients or their legal guardians.

From May 2014 to October 2016, 90 patients with brain tumours who had not received chemotherapy, steroid treatment or stereotactic biopsy were prospectively evaluated by conventional and whole brain advanced diffusion-weighted images (DWI). All cases of pathologically confirmed gliomas were included in our study, and the exclusion criteria were as follows: a) the acquired MRI images had serious artefacts that could affect accurate diagnosis; b) the tumour volume was < 20 $mm^3$; c) the patient had recurrent gliomas. After exclusion, 42 patients (male: 23; female: 19; age range: 13–76 years; mean age: 44.5 years) were included in the study. Among them, 18 patients with low-grade gliomas (LGGs) and 24 patients had high-grade gliomas (HGGs). The detailed pathological results are presented in Table 1. All the tumours were resected three weeks after MRI examination, and the relevant clinical information was collected.

**Table 1**
The clinical information of included patients.

| Index | High grade gliomas | | Low grade gliomas | *P* |
|---|---|---|---|---|
| | Grade IV * (n = 16) | Grade III # (n = 8) | Grade II & (n = 18) | |
| Age (mean, year) | 51.8 | 46.5 | 37.2 | 0.011 |
| Sex (male) | 9 | 2 | 12 | 0.171 |
| *IDH-1* | | | | |
| *IDH-1* (+) | 4 | 7 | 12 | 0.005 |
| *IDH-1* (−) | 12 | 1 | 5$ | |
| Ki-67 | 0.37 | 0.22 | 0.04$ | < 0.001 |

*: Glioblastoma, *IDH-1* mutant (n = 4); Glioblastoma *IDH-1* wild type (n = 12).
#: Anaplastic astrocytoma, *IDH-1* mutant (n = 1); Anaplastic oligodentroglioma NOS (n = 3); Oligodentroglioma NOS (n = 3); Oligodentroglioma *IDH-1* mutant and 1p/19q codeleted (n = 1).
&: Diffuse astrocytoma, *IDH-1* mutant (n = 7); Diffuse astrocytoma, *IDH-1* wild type (n = 4); Diffuse astrocytoma NOS (n = 1); Oligodentroglioma NOS (n = 6).
$: one patient with grade II glioma without the specific gene examination result.

### 2.2. MRI protocol and data post-processing

#### 2.2.1. Conventional MRI

Brain MRI was performed on all patients using a 3T MR system (Magnetom Verio, Siemens Medical Solutions, Erlangen, Germany) with 12 phased-array head coils. Transversal T2-weighted images (repetition time (TR): 4000 ms; echo time (TE): 100 ms; field of view (FOV): 230 mm × 230 mm; slice thickness: 5 mm; slice gap: 0.5 mm; voxel resolution: 0.7 mm × 0.6 mm × 6.0 mm), transversal T1-weighted images (TR: 400 ms; TE: 8.9 ms; FOV: 230 mm × 230 mm; slice thickness: 5 mm; slice gap: 0.5 mm; voxel resolution: 0.9 mm × 0.7 mm × 6.0 mm) and coronary fluid-attenuated inversion recovery images (TR/TE: 9000 ms/110 ms; inversion time: 2500 ms; FOV: 260 mm × 260 mm; slice thickness: 5 mm; slice gap: 0.5 mm; voxel resolution: 0.9 mm × 0.7 mm × 6.0 mm) were obtained. Post-contrast sagittal 3D T1-weighted images (TR: 1880 ms; TE: 2.62 ms; section thickness: 1 mm; FOV: 256 mm × 256 mm; voxel resolution: 0.7 mm × 0.7 mm × 0.7 mm) were obtained after whole brain advanced DWI imaging. Contrast media (0.1 mmol/kg body weight of Gd-DTPA, Magnevist, Schering, Berlin, Germany) was injected at a rate of 2 ml/s, followed by a 20-ml 0.9% saline flush using the same injection speed.

#### 2.2.2. Whole brain advanced DWI

The Echo planar imaging (EPI) diffusion-weighted data were acquired along 30 diffusion gradient directions, with three b values (0, 1000, and 2000 s/$mm^2$) for each direction. The sequence parameters were as follows: TR, 5500 ms; TE, 83.6 msec; FOV, 220 × 220 $mm^2$; matrix size, 110 × 110; slice thickness: 4 mm; and acquisition time, 6.3 min. All datasets were visually inspected in each orthogonal view (axial, sagittal, and coronal).

#### 2.2.3. Data processing and ROI placement

All data was transformed to nifti format. Eddy current correction was applied to diffusion data (eddy correct, FSL). Then, the corresponding NODDI metric maps, including icvf and ODI, were derived using the NODDI MATLAB Toolbox (http://www.nitrc.org/projects/noddi_toolbox). Diffusion-weighted images with b = 0 and 1000 s/$mm^2$ were used for DTI fitting. A map of mean diffusion (MD) and fractional anisotropy (FA) was calculated using DKE software (Diffusion Kurtosis Estimator, http://www.nitrc.org/projects/dke).

All the NODDI, DTI metrics, and $T_1$WI enhancement maps were co-

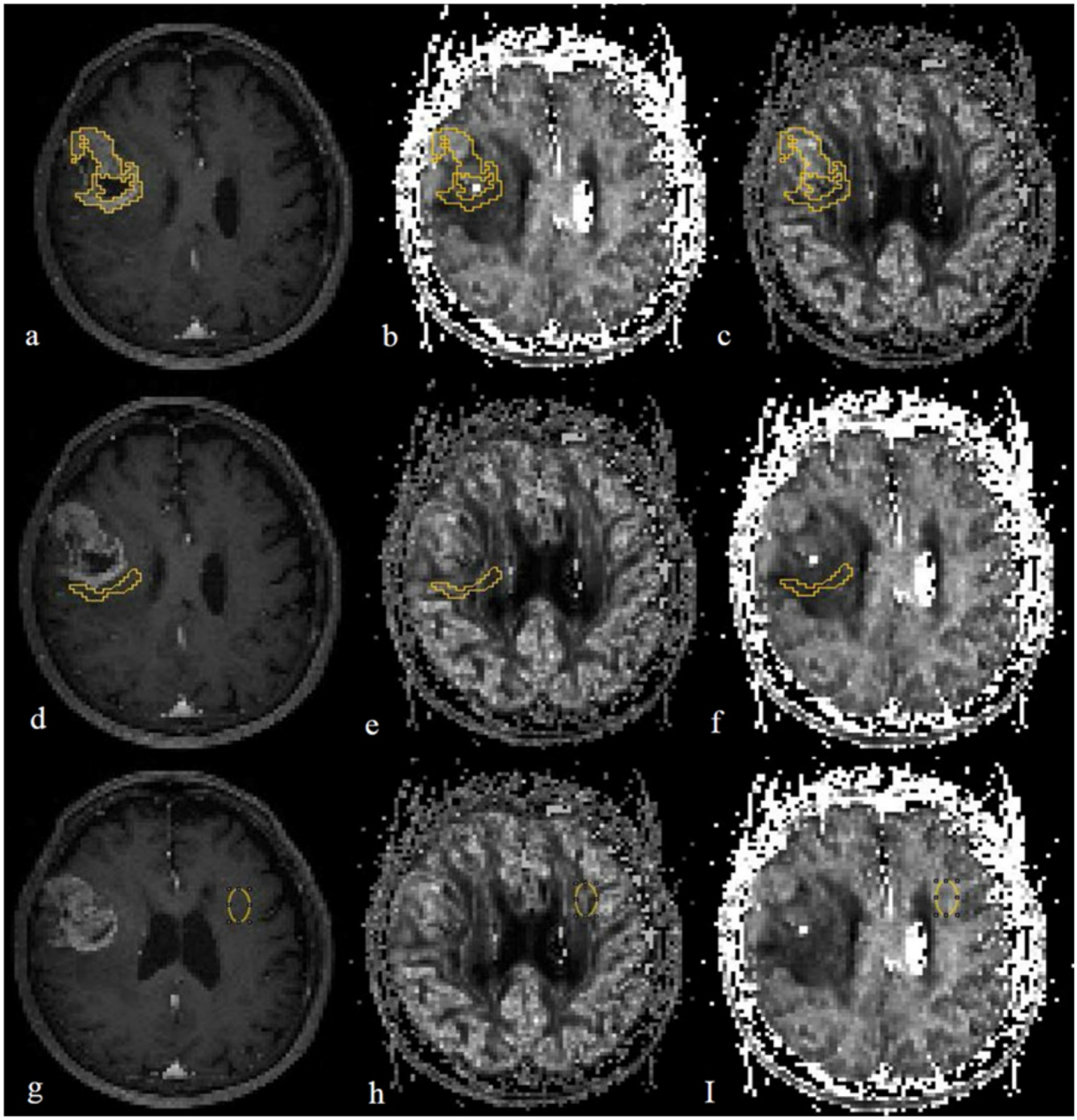


**Fig. 1.** An example of putting the ROIs in a co-registrated enhanced T1 weighted image (a, d, g), intracellular volume fraction (icvf: b, e, h) and orientation dispersion index (ODI: c, f, I) maps, respectively. a, b, c: in tumour parenchyma, ROI was designed to be as large as possible to cover the tumour parenchyma; d, e, f: ROI was within 1 cm from the outer enhancing tumour margin in peritumoural area; g, h, i: ROI was placed in contralateral normal-appearing white matter.

registered via voxel-based nonlinear registration methods using SPM 8 (Statistical Parametric Mapping, London, UK, http://www.fil.ion.ucl.ac.uk/spm). ROIs were drawn in ImageJ (Version 1.46r, NIH, USA) based on the consensus of two experienced radiologists. According to fluid attenuated inversion recovery (FLAIR) and contrast enhanced $T_1$ weighted images, three ROIs were placed on tumour parenchyma (TP), peritumoural area (PT) and contralateral normal-appearing white matter (NAWM) regions, avoiding the necrosis and cystic component (Fig. 1). The PT area was defined by the following parameters: a) if the tumour was obviously enhanced according to enhanced $T_1$ weighted images, the PT area was considered to be within 1 cm from the outer enhancing tumour margin; b) if the tumour was without obvious enhancement, according to FLAIR images, the PT area was considered to be within 1 cm from the relatively higher signal delineated tumour margin. The size of the ROI in TP regions was designed as large as possible in order to cover the tumour parenchyma, and in PT or NAWM area, it was similar to each other in each tumour (Fig. 1). The mean values of icvf, ODI, MD and FA in TP, PT and NAWM regions were recorded, and the mean ratio values of TP to NAWM on icvf (ricvf) and ODI (rODI) maps were calculated as well.

To determine the test-retest reliability of NODDI parameters in our study, a neuroradiologist used the aforementioned method to delineate the ROIs in 26 randomly selected patients.

### 2.2.4. *Pathology and immunohistochemistry analysis*

The nature and grade of the gliomas was determined according to the 2016 WHO classification (Louis et al., 2016). Immunohistochemical staining for Ki-67 was performed using the Envision method (Clone No. UMAB107, dilution 1:300). The tumour sections were reviewed and quantified based on the percentage of positive cells in the highest density staining area; all cells with nuclear staining of any intensity were considered positive, and the Ki-67 values were defined as the

percentage of positive cells among the total cells counted (Alexiou et al., 2014).

### 2.3. Statistical analysis

Statistical analysis was performed using SPSS (SPSS 20.0 Chicago). The demographic characteristics and differences between tumour grading were analysed by a Chi-square test or one-way ANOVA when appropriate. The associations between parameters of quantitative NODDI and DTI metrics and glioma grading were evaluated by univariate and multivariate stepwise logistic regression models. Receiver operating characteristic (ROC) curves were constructed to assess the diagnostic efficiency of NODDI and DTI parameters on glioma grading, and the area under the curve (AUC) along with the 95% CI was derived. The optimal cut-off value for a continuous variable being transformed into a binary variable was defined as the point on the ROC curve that maximized the Youden index. Sensitivity, specificity and accuracy were calculated. The intra-examiner consistency was assessed by interclass correlation coefficients (ICC). The associations between quantitative NODDI metrics and Ki-67 were assessed by Spearman correlation coefficients. A $P < 0.05$ was considered statistically significant.

## 3. Results

### 3.1. Patients

Information about *IDH-1* mutation screening and Ki-67 values was available for 41 of the 42 patients included in this study. The detailed information is shown in Table 1 and Fig. 2. No gender differences were found among the different grades of gliomas. Overall, the patient age increased as glioma grade increased. The age difference between the grade IV and II patients was statistically significant ($P = 0.002$). However, the incidence of *IDH-1* mutation decreased as glioma grade increased.

### 3.2. The interclass correlation coefficients of NODDI metrics

The interclass correlation coefficients of the test-retest reliability for NODDI parameters in our study ranged from 0.591 and 0.991 ($icvf_{TP}$: 0.991, 95% CI: 0.979–0.996; $ODI_{TP}$: 0.978, 95% CI: 0.951–0.990; $icvf_{NAWM}$: 0.591, 95% CI: 0.087–0.816; $ODI_{NAWM}$: 0.854, 95% CI: 0.673–0.934; $icvf_{PT}$: 0.881, 95% CI: 0.734–0.947; $ODI_{PT}$: 0.842, 95% CI: 0.648–0.929). The intra-examiner reliability for all parameters was generally acceptable.

### 3.3. Diagnostic performance of NODDI and DTI metrics for grading gliomas

The univariate analysis showed that, in TP, the mean value of icvf, ODI and FA was significantly higher in HGGs compared to LGGs, while the mean value of MD was significantly lower in HGGs. Furthermore, in the PT area, the mean value of icvf and FA was significantly lower in HGGs, while the mean value of MD was significantly higher in HGGs (Fig. 3). No significant differences were observed in icvf, ODI and DTI metrics of NAWM between HGGs and LGGs patients. Further, comparing the mean ratio values of icvf and ODI between HGGs and LGGs, we found that the ratio of icvf and ODI was significantly higher in HGGs than LGGs. ROC curves showed that the icvf in the TP area demonstrated a significant diagnostic value for grading gliomas (AUC: 0.81, 95% CI: 0.66–0.95), and the specificity, sensitivity and accuracy of optimal cut-off values (0.31) were 78%, 88% and 83%, respectively (Tables 2 and 3).

The multivariate stepwise logistic regression showed that age (OR = 1.104) and icvf values in TP (OR = 12.169) and PT areas (OR = 11.654) were statistically significantly associated with tumour grading. The comprehensive score generated from the logistic regression model ($Score = -6.149 + 0.099 * age + 2.499 * icvf_{TP} + 2.456 * icvf_{PT}$) showed a high discrimination value for grading gliomas (AUC = 0.92, $P < 0.001$). The optimal cut-off value for the score was 0.59, and the corresponding sensitivity, specificity and accuracy were 92%, 89% and 91%, respectively (Table 4) (Fig. 4). Further analysis showed that tumours with high icvf values in TP ($\geq 0.306$) and low icvf values in the PT area ($\leq 0.331$) were more likely to be HGGs, while lesions with low icvf values in TP ($< 0.306$) and higher icvf values in PT ($> 0.331$) were likely to be LGGs ($P < 0.001$) (Table 5).

In addition to differentiating between HGGs and LGGs, the differences among grade II, III and IV gliomas were further compared. Compared to grade II gliomas, the icvf in TP and MD in the PT area were significantly higher in grade III gliomas (TP: $icvf_{II}$ vs. $icvf_{III} = 0.246 \pm 0.130$ vs. $0.403 \pm 0.135$; $P = 0.011$; PT: $MD_{II}$ vs. $MD_{III} = (1.085 \pm 0.229) \times 10^{-3}\,mm^2/s$ vs. $(1.547 \pm 0.444) \times 10^{-3}\,mm^2/s$; $P = 0.005$). Similarly, the ricvf and rODI were also significantly higher in grade III gliomas ($ricvf_{II}$ vs. $ricvf_{III} = 0.437 \pm 0.242$ vs. $0.697 \pm 0.259$; $P = 0.028$; $rODI_{II}$ vs. $rODI_{III} = 1.295 \pm 0.498$ vs.$1.823 \pm 0.720$; $P = 0.035$). ROC analysis showed that icvf in TP had the highest diagnostic value (AUC: 0.82) and the sensitivity, specificity and cut-off value were 88%, 72% and 0.26, respectively. However, no significant differences were found in NODDI and DTI metrics to discriminate grade IV from grade III gliomas.

### 3.4. Diagnostic performance of NODDI and DTI metrics for IDH-1 mutation detection

Irrespective of the glioma grade, there were no significant differences in NODDI (Fig. 2) and DTI metrics to differentiate *IDH-1*-positive from *IDH-1*-negative patients (Table 2).

Furthermore, the correlations between *IDH-1* mutation status and NODDI metrics were sub-analysed within each grade of glioma. For grade IV gliomas, the mean value of ricvf was significantly higher in patients with *IDH-1* mutations ($ricvf_{IDH\text{-}1(+)}$ vs. $ricvf_{IDH\text{-}1(-)}$: $0.971 \pm 0.106$ vs. $0.751 \pm 0.238$; $P = 0.029$). The ROC curve for ricvf demonstrated that the diagnostic value, sensitivity, specificity and cut-off values were 0.88, 100%, 75% and 0.84, respectively. For grade

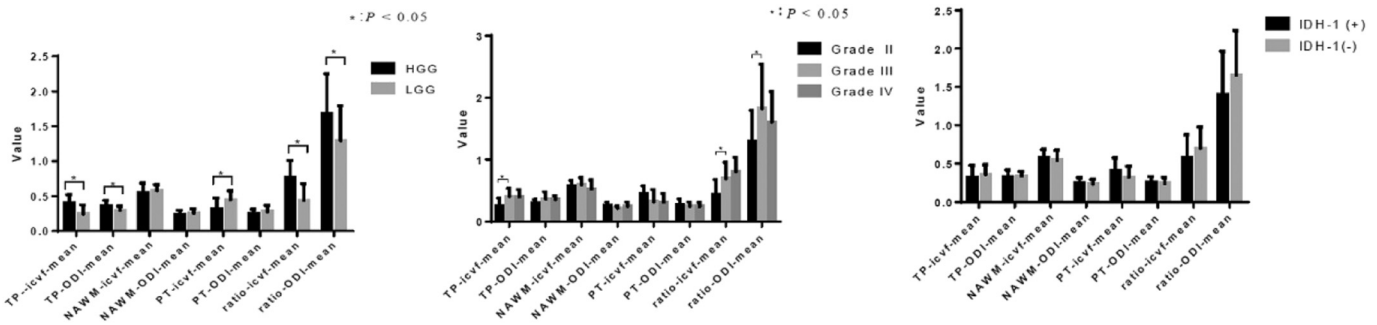


**Fig. 2.** Statistic description maps (mean ± SD) of the included patients with the different grades of gliomas and different IDH-1 mutation statuses.

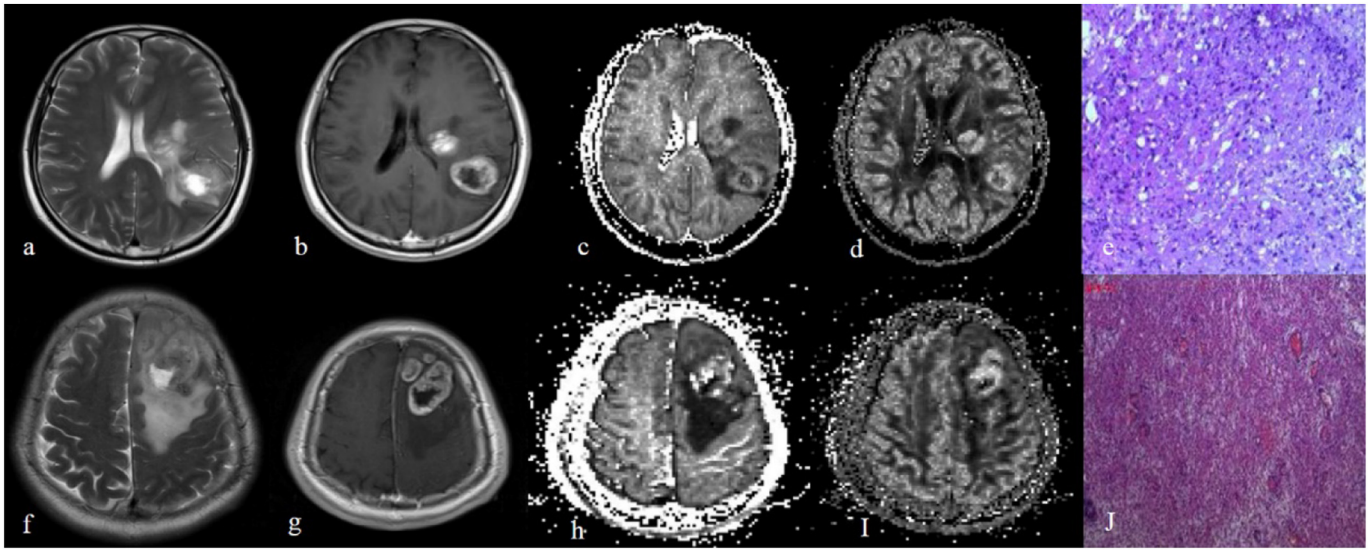


**Fig. 3.** Upper images (a, b, c, d, e) show a 51-year-old male with low grade gliomas (e, pathologically confirmed gemistocytic astrocytoma, haematoxylin-Eosin (HE) × 10) which mainly is located in left temporal lobe and left basal ganglia region. Lower images (f, g, h, i, j) demonstrate a 61-year-old male with high grade gliomas (j, pathologically proved as glioblastoma, haematoxylin-Eosin (HE) × 10) in the left frontal lobe. Both tumours had obvious necrosis on T2 weighted images (a, f) and the tumour parenchyma showed vivid enhancement (b, g); however, the higher-grade glioma showed slightly higher ODI value (d, i) and, further, the icvf map (c, h) showed that high grade glioma with higher icvf value in tumour parenchyma.

**Table 2**
Comparison of NODDI and DTI parameters between groups for tumour differentiation and *IDH-1* status.

| Variables | Tumour differentiation | | | *IDH-1* status | | |
|---|---|---|---|---|---|---|
| | LGG (n = 18) | HGG (n = 24) | *P* | Negative (n = 18) | Positive (n = 23) | *P* |
| TP | | | | | | |
| icvf | 0.246 ± 0.130 | 0.401 ± 0.119 | < 0.001 | 0.357 ± 0.128 | 0.322 ± 0.159 | 0.441 |
| ODI | 0.299 ± 0.058 | 0.360 ± 0.078 | 0.009 | 0.340 ± 0.058 | 0.327 ± 0.089 | 0.591 |
| FA | 0.138 ± 0.041 | 0.174 ± 0.049 | 0.015 | 0.171 ± 0.050 | 0.152 ± 0.046 | 0.208 |
| MD ($\times 10^{-3}$ mm$^2$/s) | 1.609 ± 0.321 | 1.299 ± 0.272 | 0.002 | 1.379 ± 0.345 | 1.461 ± 0.321 | 0.436 |
| PT | | | | | | |
| icvf | 0.448 ± 0.130 | 0.315 ± 0.155 | 0.006 | 0.321 ± 0.142 | 0.410 ± 0.165 | 0.075 |
| ODI | 0.278 ± 0.089 | 0.245 ± 0.065 | 0.180 | 0.243 ± 0.074 | 0.262 ± 0.067 | 0.402 |
| FA | 0.284 ± 0.088 | 0.212 ± 0.088 | 0.012 | 0.228 ± 0.074 | 0.259 ± 0.108 | 0.309 |
| MD ($\times 10^{-3}$ mm$^2$/s) | 1.085 ± 0.229 | 1.458 ± 0.373 | 0.001 | 1.373 ± 0.327 | 1.251 ± 0.398 | 0.301 |
| TP/NAWM | | | | | | |
| icvf | 0.437 ± 0.242 | 0.770 ± 0.241 | < 0.001 | 0.701 ± 0.279 | 0.576 ± 0.300 | 0.179 |
| ODI | 1.295 ± 0.498 | 1.679 ± 0.571 | 0.028 | 1.658 ± 0.578 | 1.404 ± 0.561 | 0.164 |

TP: tumour parenchyma; PT: peritumoural area; NAWM: normal-appearing white matter; icvf: intracellular volume fraction; ODI: orientation dispersion index; FA: fractional anisotropy; MD: mean diffusion.

**Table 3**
Univariate, the area under the curves, the optimal cutoff values, and corresponding sensitivities and specificities based on ROC curves in grading gliomas.

| Variables | Cut-off value | Sensitivity | Specificity | AUC (95% CI) | *P* |
|---|---|---|---|---|---|
| NODDI parameter | | | | | |
| TP icvf | 0.306 | 0.875 | 0.778 | 0.806 (0.660, 0.952) | 0.001 |
| TP ODI | 0.338 | 0.583 | 0.833 | 0.723 (0.569, 0.878) | 0.014 |
| PT icvf | 0.331 | 0.625 | 0.889 | 0.731 (0.573, 0.890) | 0.011 |
| DTI parameter | | | | | |
| TP FA | 0.161 | 0.667 | 0.778 | 0.730 (0.574, 0.887) | 0.011 |
| TP MD | 1.600 | 0.958 | 0.444 | 0.731 (0.577, 0.886) | 0.011 |
| PT FA | 0.199 | 0.542 | 0.833 | 0.718 (0.561, 0.874) | 0.017 |
| PT MD | 1.210 | 0.750 | 0.889 | 0.775 (0.625, 0.926) | 0.002 |

TP: tumour parenchyma; PT: peritumoural area; icvf: intracellular volume fraction; ODI: orientation dispersion index; FA: fractional anisotropy; MD: mean diffusion ($\times 10^{-3}$ mm$^2$/s).

**Table 4**
The results of multivariate stepwise logistic regression analysis.

| Variable | *b* | *Beta* | OR (95% CI) | *P* |
|---|---|---|---|---|
| Constant | −6.419 | – | – | 0.005 |
| Age (year) | 0.099 | 0.075 | 1.104 (1.016, 1.200) | 0.020 |
| TP icvf | | | | |
| Low (< 0.306) | | | 1 | |
| High (≥0.306) | 2.499 | 0.684 | 12.169 (1.636, 90.527) | 0.015 |
| PT icvf | | | | |
| High (> 0.331) | | | 1 | |
| Low (≤0.331) | 2.456 | 0.673 | 11.654 (1.205, 112.692) | 0.034 |

TP: tumour parenchyma; PT: peritumoural area.

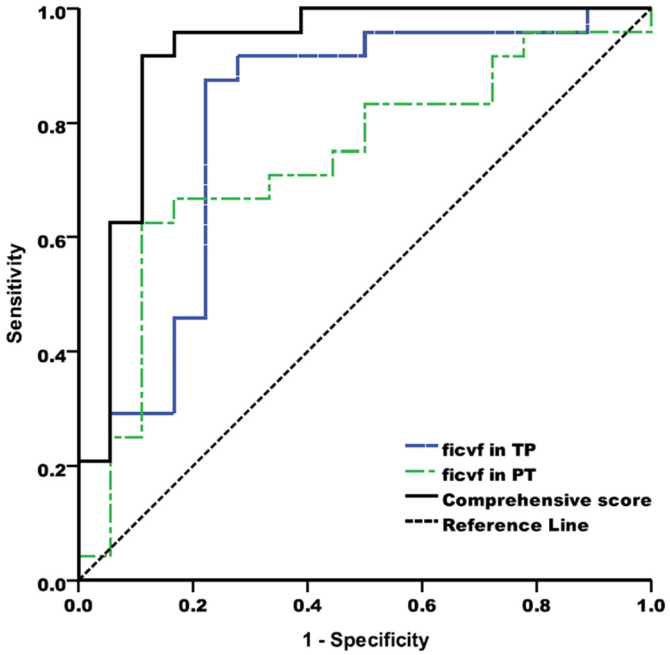


**Fig. 4.** ROC curves for $icvf_{TP,}$ $icvf_{PT}$ and the combining analysis of the regression equation (Score = $-6.149 + 0.099 * age + 2.499 * icvf_{TP} + 2.456 * icvf_{PT}$) which demonstrated the highest discrimination value for grading gliomas (AUC = 0.92, $P < 0.001$).

**Table 5**
Group analysis of the patients with different icvf values in different tumour area.

| Group | LGG (n = 18) | HGG (n = 24) | Total | *P* |
|---|---|---|---|---|
| TP icvf = N & PT icvf = N | 13 (87%) | 2 (13%) | 15 | < 0.001 |
| TP icvf = N & PT icvf = P | 1 (50%) | 1 (50%) | 2 | |
| TP icvf = P & PT icvf = N | 3 (30%) | 7 (70%) | 10 | |
| TP icvf = P & PT icvf = P | 1 (7%) | 14 (93%) | 15 | |

TP: tumour parenchyma; PT: peritumoural area.
The values for TP and PT icvf were determined by regression analysis (TP icvf: N = " < 0.306", P = "≥0.306"; PT icvf: N = " > 0.331", P = "≤0.331").

II gliomas, the NODDI and DTI parameters were not statistically significant for the detection of IDH mutations.

### 3.5. Correlation between NODDI metrics and Ki-67

The difference in Ki-67 expression between HGGs and LGGs was significant ($P < 0.001$). The difference in Ki-67 expression among grade II, III and IV gliomas were also significant ($P < 0.001$), and this held true for any pairwise analysis ($P \leq 0.023$). The Ki-67 expression was significantly higher in higher-grade gliomas.

In the TP region, significantly positive correlations were found between Ki-67 expression and icvf and Ki-67 expression and ODI (icvf: $r = 0.429$, $P = 0.004$; ODI: $r = 0.530$, $P < 0.001$), while the icvf in the PT area was inversely correlated with Ki-67 expression ($r = -0.498$, $P = 0.003$). The correlation coefficient for ODI was higher than that for icvf (the corresponding scatter diagrams are shown in Fig. 5).

## 4. Discussion

For HGGs, NODDI metrics were significantly higher in the TP region, while the mean value of icvf was significantly lower in the PT region. The icvf value could significantly differentiate grade II from III gliomas. Combining the variables of patient age and mean values of icvf in the TP and PT areas yielded the highest diagnostic performance for grading gliomas. Furthermore, for grade IV gliomas, the mean value of ricvf was significantly higher in *IDH-1*-positive patients.

NODDI was developed based on the hindered and restricted diffusion models (Assaf & Cohen, 2000). Hindered diffusion characterizes the water in the extra-cellular space as defined by the cellular membranes of somas and glial cells (Zhang et al., 2012). Restricted diffusion refers to the diffusion of water in restricted geometries, and it describes the water in the intra-cellular space bounded, for example, by axonal or dendritic membranes (Zhang et al., 2012). Glioma is characterized by varying degrees of hypercellularity, nuclear pleomorphism, endothelial proliferation and microvascular density. All these transformations will replace normal brain tissue and infiltrate adjacent brain tissue, resulting in alterations in the brain microenvironment. Compared with NAWM, gliomas cause axonal and neuronal fibre projection disruption, resulting in reduced intracellular diffusivity, which leads to a lower icvf value. The ODI was higher for glioma than for NAWM, which could be explained by the tumour tissue tending to be isotropic due to neuronal fibre disruption.

HGGs, compared with LGGs, have a higher degree of cellularity, nuclear pleomorphism, endothelial proliferation and microvascular density, which could highly restrict the movement of water molecules via hindered and restricted diffusion. Therefore, HGGs are expected to have a higher icvf value than LGGs. Similarly, in HGGs, the destruction of normal brain tissue is more obvious than in LGGs, and it is prone to be more isotropic, resulting in a higher ODI value. Our results were in accordance with this hypothesis. In addition, we analysed the correlation of Ki-67 expression with NODDI metrics. Ki-67 expression was used to predict cellular proliferation (Habberstad et al., n.d.; Donato et al., 2007). Our results indicate that significantly higher cellular proliferation levels are found in HGGs, and the mean value of icvf and ODI are significantly positively correlated with the Ki-67 values in TP. This result is also consistent with our hypothesis. We might also infer that this proliferation could be non-invasively predicted by NODDI metrics.

On the other hand, HGGs grow in a more aggressive manner than LGGs and infiltrate adjacent brain tissue (Walker et al., 2011). The tumour infiltration but not replace the brain parenchyma could affect the integrity of normal brain tissue, which would decrease hindered and restricted diffusion in peritumoural areas. Therefore, we assumed that the icvf of HGGs is lower than LGGs in the PT area. Furthermore, the icvf of LGGs was lower than contralateral NAWM. Our results did show a similar tendency, and the mean value of icvf in the PT area was significantly lower in HGGs than in LGGs.

A variety of studies using DTI and DKI for grading gliomas have shown that DKI is a better diagnostic tool than DTI, and MK is the best independent predictor for stratifying glioma grades (Van Cauter et al., 2012). Our results also indicate that NODDI parameters are superior to DTI metrics in grading gliomas. In the present study, we did not compare the diagnostic efficacy of DKI and NODDI for differentiation of glioma grade. However, compared with a newly published meta-analysis of the utility of DKI for grading gliomas (Falk Delgado et al., n.d.), the multivariate logistic regression model with NODDI metrics in our study showed comparable diagnostic value and similar sensitivity and

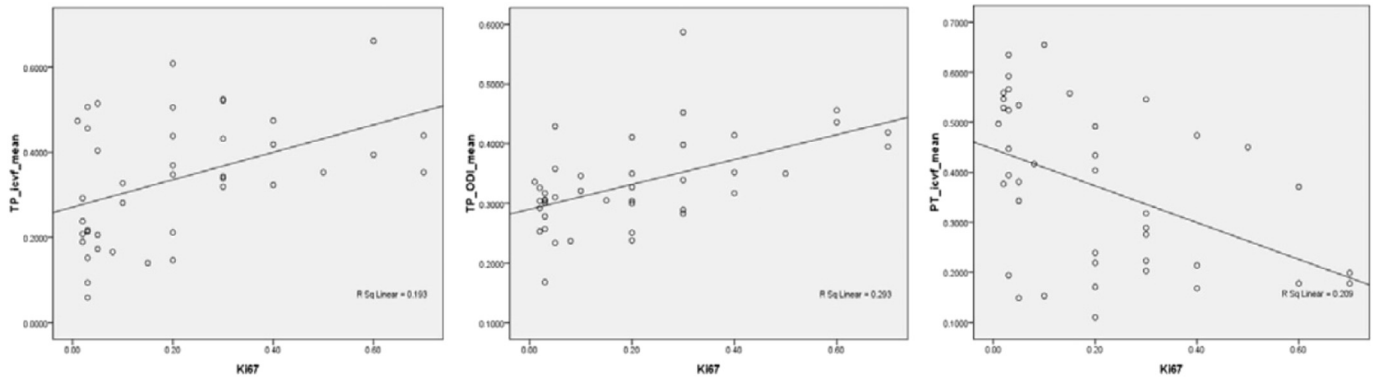


**Fig. 5.** Scatter diagrams of NODDI metrics with Ki-67. a, b, Ki-67 expression was significantly positively correlated with icvf and ODI in the tumour parenchyma and c, Ki-67 expression was inversely correlated with icvf in the peritumoural area.

specificity. Restricted spectrum imaging (RSI) is an advanced DWI modelling technique that enables quantitative estimates of nuclear volume fraction. However, it was not widely available. Several studies (White et al., n.d.; Kothari et al., 2013; McDonald et al., 2016) have focused on tumour response monitoring and HGG margin delineation, but RSI has rarely been applied for grading gliomas.

Furthermore, recent studies on the identification of *IDH-1* mutation status by DTI (Xiong et al., 2016) and DKI (Hempel et al., 2017b) have shown that *IDH-1*-mutated gliomas have lower maximum FA and mean MK values. The authors hypothesized that lower FA and MK values represent more homogeneous cellular architecture and lower cell density (Beppu et al., 2005; Kinoshita et al., 2008; Popov et al., 2013). However, our study demonstrated that, in grade IV gliomas, the mean value of ricvf is significantly higher in *IDH-1* positive patients. The icvf is positively correlated with tumour cellularity, which contradicts the aforementioned results from DTI and DKI. Our results still need be further applied to larger data sets.

Our study has three main limitations. First, our results show that the utility of NODDI metrics in detecting *IDH-1* mutation status has not been fully established, as a larger group size may demonstrate benefits. Second, since gliomas are heterogeneous tumours and the immunohistological sections were not registered with the ROIs, the ROI-based method might cause some bias, especially in HGGs. Moreover, our direction setting of diffusion gradient and voxel size may be not optimized for the NODDI model. While we used this setting because it is widely available for clinical scanner and feasible for routine MR exam.

## 5. Conclusions

As a new diffusion MRI technique, NODDI shows great potential for glioma grading. It is promising that the regression model utilizing age and icvf values has a very high ability to predict glioma grade. However, the utility of NODDI in detecting *IDH-1* mutation status has not been established due to small group size. Furthermore, NODDI metrics might offer great potential for providing additional information on the cellular proliferation of gliomas.

## Acknowledgement

This study was supported by National Natural Science Foundation of China (81201074) and Fundamental Research Funds for the Central Universities (13ykpy14).

## References

Adluru, G., Gur, Y., Anderson, J.S., et al., 2014. Assessment of white matter microstructure in stroke patients using NODDI. Conf. Proc. IEEE Eng. Med. Biol. Soc. 2014, 742–745.

Alexiou, G.A., Zikou, A., Tsiouris, S., et al., 2014. Correlation of diffusion tensor, dynamic susceptibility contrast MRI and (99m) Tc-Tetrofosmin brain SPECT with tumour grade and Ki-67 immunohistochemistry in glioma. Clin. Neurol. Neurosurg. 116, 41–45.

Andronesi, O.C., Rapalino, O., Gerstner, E., et al., 2013. Detection of oncogenic IDH1 mutations using magnetic resonance spectroscopy of 2-hydroxyglutarate. J. Clin. Invest. 123, 3659–3663.

Assaf, Y., Cohen, Y., 2000. Assignment of the water slow-diffusing component in the central nervous system using q-space diffusion MRS: implications for fiber tract imaging. Magn. Reson. Med. 43, 191–199.

Bai, Y., Lin, Y., Tian, J., et al., 2016. Grading of gliomas by using monoexponential, biexponential, and stretched exponential diffusion-weighted MR imaging and diffusion kurtosis MR imaging. Radiology 278, 496–504.

Beppu, T., Inoue, T., Shibata, Y., et al., 2005. Fractional anisotropy value by diffusion tensor magnetic resonance imaging as a predictor of cell density and proliferation activity of glioblastomas. Surg. Neurol. 63, 56–61.

Bertolino, N., Marchionni, C., Ghielmetti, F., et al., 2014. Accuracy of 2-hydroxyglutarate quantification by short-echo proton-MRS at 3 T: a phantom study. Phys. Med. 30, 702–707.

Donato, V., Papaleo, A., Castrichino, A., et al., 2007. Prognostic implication of clinical and pathologic features in patients with glioblastoma multiforme treated with concomitant radiation plus temozolomide. Tumori 93, 248–256.

Falk Delgado, A., Nilsson, M., van Westen, D., Falk Delgado, A., 2017. Glioma grade discrimination with MR diffusion kurtosis imaging: a meta-analysis of diagnostic accuracy. Radiology 287 (1), 119–127 (171315).

Goodenberger, M.L., Jenkins, R.B., 2012. Genetics of adult glioma. Cancer Genet. 205, 613–621.

Habberstad, A.H., Gulati, S., Torp, S.H., 2011. Evaluation of the proliferation markers Ki-67/MIB-1, mitosin, survivin, pHH3, and DNA topoisomerase IIalpha in human anaplastic astrocytomas–animmunohistochemical study. Diagn. Pathol. 24 (6), 43.

Hartmann, C., Meyer, J., Balss, J., et al., 2009. Type and frequency of IDH1 and IDH2 mutations are related to astrocytic and oligodendroglial differentiation and age: a study of 1,010 diffuse gliomas. Acta Neuropathol. 118, 469–474.

Hartmann, C., Hentschel, B., Wick, W., et al., 2010. Patients with IDH1 wild type anaplastic astrocytomas exhibit worse prognosis than IDH1-mutated glioblastomas, and IDH1 mutation status accounts for the unfavorable prognostic effect of higher age: implications for classification of gliomas. Acta Neuropathol. 120, 707–718.

Hempel, J.M., Bisdas, S., Schittenhelm, J., et al., 2017a. In vivo molecular profiling of human glioma using diffusion kurtosis imaging. J. Neuro-Oncol. 131 (1), 93–101.

Hempel, J.M., Schittenhelm, J., Brendle, C., et al., 2017b. Histogram analysis of diffusion kurtosis imaging estimates for in vivo assessment of 2016 WHO glioma grades: a cross-sectional observational study. Eur. J. Radiol. 95, 202–211.

Kamagata, K., Hatano, T., Okuzumi, A., et al., 2016. Neurite orientation dispersion and density imaging in the substantia nigra in idiopathic Parkinson disease. Eur. Radiol. 26, 2567–2577.

Kickingereder, P., Sahm, F., Radbruch, A., et al., 2015. IDH mutation status is associated with a distinct hypoxia/angiogenesis transcriptome signature which is non-invasively predictable with rCBV imaging in human glioma. Sci. Rep. 5, 16238.

Kinoshita, M., Hashimoto, N., Goto, T., et al., 2008. Fractional anisotropy and tumor cell density of the tumor core show positive correlation in diffusion tensor magnetic resonance imaging of malignant brain tumors. NeuroImage 43, 29–35.

Kothari, P.D., White, N.S., Farid, N., et al., 2013. Longitudinal restriction spectrum imaging is resistant to pseudoresponse in patients with high-grade gliomas treated with bevacizumab. AJNR Am. J. Neuroradiol. 34, 1752–1757.

Lee, S., Choi, S.H., Ryoo, I., et al., 2015. Evaluation of the microenvironmental heterogeneity in high-grade gliomas with IDH1/2 gene mutation using histogram analysis of diffusion-weighted imaging and dynamic-susceptibility contrast perfusion imaging. J. Neuro-Oncol. 121, 141–150.

Louis, D.N., Perry, A., Reifenberger, G., et al., 2016. The 2016 World Health Organization Classification of Tumors of the Central Nervous System: a summary. Acta Neuropathol. 131, 803–820.

McDonald, C.R., Delfanti, R.L., Krishnan, A.P., et al., 2016. Restriction spectrum imaging predicts response to bevacizumab in patients with high-grade glioma. Neuro-Oncology 18, 1579–1590.

Popov, S., Jury, A., Laxton, R., Doey, L., Kandasamy, N., Al-Sarraj, S., et al., 2013. IDH1-associated primary glioblastoma in young adults displays differential patterns of tumour and vascular morphology. PLoS ONE 8, e56328.
Tropine, A., Vucurevic, G., Delani, P., et al., 2004. Contribution of diffusion tensor imaging to delineation of gliomas and glioblastomas. J. Magn. Reson. Imaging 20, 905–912.
Van Cauter, S., Veraart, J., Sijbers, J., et al., 2012. Gliomas: diffusion kurtosis MR imaging in grading. Radiology 263 (2), 492–501.
Walker, C., Baborie, A., Crooks, D., et al., 2011. Biology, genetics and imaging of glial cell tumours. Br. J. Radiol. 84, S90–106.
Weiler, M., Wick, W., 2012. Molecular predictors of outcome in low-grade glioma. Curr. Opin. Neurol. 25, 767–773.
Weller, M., Pfister, S.M., Wick, W., et al., 2013. Molecular neurooncology in clinical practice: a new horizon. Lancet Oncol. 14, e370–9.
Wen, Q., Kelley, D.A., Banerjee, S., et al., 2015. Clinically feasible NODDI characterization of glioma using multiband EPI at 7 T. Neuroimage Clin 9, 291–299.
White, N.S., McDonald, C., Farid, N., et al., 2014. Diffusion-weighted imaging in cancer: physical foundations and applications of restriction spectrum imaging. Cancer Res. 74, 4638–4652.
White, N.S., McDonald, C.R., Farid, N., Kuperman, J.M., Kesari, S., Dale, A.M., 2013. Improved conspicuity and delineation of high-grade primary and metastatic brain tumors using “restriction spectrum imaging”: quantitative comparison with high B-value DWI and ADC. AJNR Am J Neuroradiol. 34, 958–964 (S1).
Winston, G.P., Micallef, C., Symms, M.R., et al., 2014. Advanced diffusion imaging sequences could aid assessing patients with focal cortical dysplasia and epilepsy. Epilepsy Res. 108, 336–339.
Xiong, J., Tan, W.L., Pan, J.W., et al., 2016. Detecting isocitrate dehydrogenase gene mutations in oligodendroglial tumors using diffusion tensor imaging metrics and their correlations with proliferation and microvascular density. J. Magn. Reson. Imaging 43 (1), 45–54.
Zhang, H., Schneider, T., Wheeler-Kingshott, C.A., et al., 2012. NODDI: practical in vivo neurite orientation dispersion and density imaging of the human brain. NeuroImage 61, 1000–1016.